Design of Very Low Profile Circular UHF Small Antenna Using Characteristic Mode Analysis

Yue Gao[1,*], Runbo Ma[2], Qianyun Zhang[1], Clive Parini[1]

[1]School of Electronic Engineering and Computer Science, Queen Mary University of London, London, United Kingdom
[2]College of Physics and Electronics Engineering, Shanxi University, Taiyuan, 030006, China
[*]E-mail: yue.gao@qmul.ac.uk

Abstract: This paper presents a very low profile circular UHF small antenna with a radiating body transformed from a monopole. The proposed radiating body is gradually improved by analyzing fundamental modes of the structure with different ground planes via characteristic mode analysis (CMA). CMAs demonstrate operating principles of the radiating body so that a magnetic feeding loop is proposed to excite the radiating body. An equivalent circuit of the radiating body and magnetic feeding loop is then established. The relationships between antenna bandwidth, and eigen value and modal significance are derived through physical insight of the CMA. A prototype of the proposed circular antenna operating at 474MHz is fabricated and measured. It has a radius of $5.2\%\lambda_c$ (λ_c is the operating wavelength), and a profile of $0.5\%\lambda_c$. The CMA of the proposed antenna with testing cable at different lengths is applied to understand the discrepancy between simulations and measurements. The analysis and performance evaluation shows that the proposed antenna can be a strong contender for compact sensors for machine-to-machine (M2M) and Internet of Things (IoT) applications.

1. Introduction

Small antennas play very important roles for wireless communication devices within limited spaces, but their performance and bandwidth are limited by the electrical size. Wheeler and Chu generally revealed the relationship between bandwidth and electrical size of small antennas [1, 2]. Sievenpiper et. al. had summarized the product of bandwidth and efficiency for 110 antenna designs published in the IEEE Transactions on Antennas and Propagation since 2010, extracted experimental validation of performance limits [3]. It is found that most antenna structures approaching the performance limits occupy 3D volumes, and are generally not low profile.

Low profile small antennas are required and developed with the boom of portable UHF communication devices built in limited area [4, 5]. A typical antenna in smart phone is small and low profile, but generally mounted on a relative large ground plane [6]. For UHF applications such as RFID tags, very low profile small antennas are necessary [7]. There are several ways to design very-low profile small antennas. A broadband UHF RFID tag was designed by considering the optimum equivalent-circuit network necessary for bandwidth broadening in single resonant tag with conjugate matching [8]. New radiating bodies were used and investigated in [9], and relatively high product of bandwidth and efficiency were realized. In addition to RFID applications at UHF frequency bands, recently devices operating at exiting UHF TV frequency bands, termed as TV white

space, have attracted much attention from regulators, academia and industry [10–12]. One of the key applications of TV white space spectrum is the machine-to-machine (M2M) communications to enable emerging Internet of Things (IoT) applications [13–16]. The small and compact sensors for M2M and IoT applications have resulted in significant challenges for small antennas at UHF TV white space frequency bands, e.g. around 480MHz. Earlier studies on a circular co-planar inverted-F antenna for M2M communications at TV white space frequency band 480MHz were presented in [17]. The size reduction was achieved by transforming a planar inverted-F antenna (PIFA). Furthermore, a printed monopole antenna was miniaturized by a magneto-dielectric superstrate for M2M Communications [18]. However, the superstrate materials are too expensive for the billions of wireless sensors required. Therefore, forming new antenna structures on a PCB for such emerging UHF M2M and IoT applications should be a promising approach to design small antennas.

Characteristic mode analysis (CMA) supported by theory of characteristic mode (TCM) becomes an attractive systematic tool to efficiently design antenna structures recently. It was proposed by Garbacz [19] and further developed by Harrington and Mautz [20, 21]. The CMA makes it possible to obtain full characteristics of a radiating body with arbitrary geometry. Based on insight in fundamental resonance characteristics of antenna geometries and structures to be mounted on, excitation locations and modes of the antenna can be optimized [22]. Several small antennas were analyzed and designed using CMA. For instance, a multiple input and multiple output (MIMO) antenna with enlarged bandwidth and single feed was realized by correlating the characteristic currents and near fields of modes with high modal significance [23]. With knowledge of characteristic modes of an electrically small unmanned aerial vehicle body, the desired currents were excited by compact and low-profile feed structures to design integrated antennas [24]. Similarly, the metallic chassis of a smart phone was excited by small coupling elements, and compact massive antenna arrays were generated by exciting multiple modes on each array element [25].

In this paper, a very low profile circular UHF small antenna is proposed. The CMA is utilized in the process of designing a radiating body and a feeding structure, establishing an equivalent circuit, estimating antenna bandwidth, and analyzing difference between results of simulation and measurement. With the physical insight from CMA, the proposed antenna ground plane is further optimized to a ring shape with an arc. The substrate is used to further reduce the size of the antenna. The equivalent circuit is established, which is used further to derive the relationship between the antenna bandwidth, and eigen value and modal significance. A prototype antenna operating at 474MHz is then fabricated, measured and connected to a sensor circuit board for performance evaluations.

The rest of this paper is organized as follows. Section II describes the proposed radiating body and characteristic mode analysis. Section III presents the magnetic feeding loop for the proposed radiating body. The equivalent circuit and bandwidth estimation methods are also established in this session. A prototype and its measurement results and analyses are presented in section IV. The conclusions are drawn in section V.

2. Radiating Body and Characteristic Mode Analysis

2.1. Proposed circular radiating body with disk ground plane

Monopoles are widely adopted for wireless communications during the last decade. It typically has a length of about $\lambda_0/4$ at resonant frequency f_0, where λ_0 is the wavelength in free space at f_0.

However, the monopole has a high profile because its pole is vertical to the ground plane. In this paper, a small radiating body with very low profile is designed by shape transformations on the monopole. The ground plane in a typical monopole is transformed into a small disk ground plane with a radius of r_3. The monopole is placed in the same plane of the disk and bent around the disk to become a circular arm with outer radius of r_1 and inner radius of r_2, as shown in Fig. 1(a). The width and average radius of the arm are $w_1 = r_1 - r_2$ and $r_0 = (r_1 + r_2)/2$, respectively. The arc between open and short end of the arm is defined as θ.

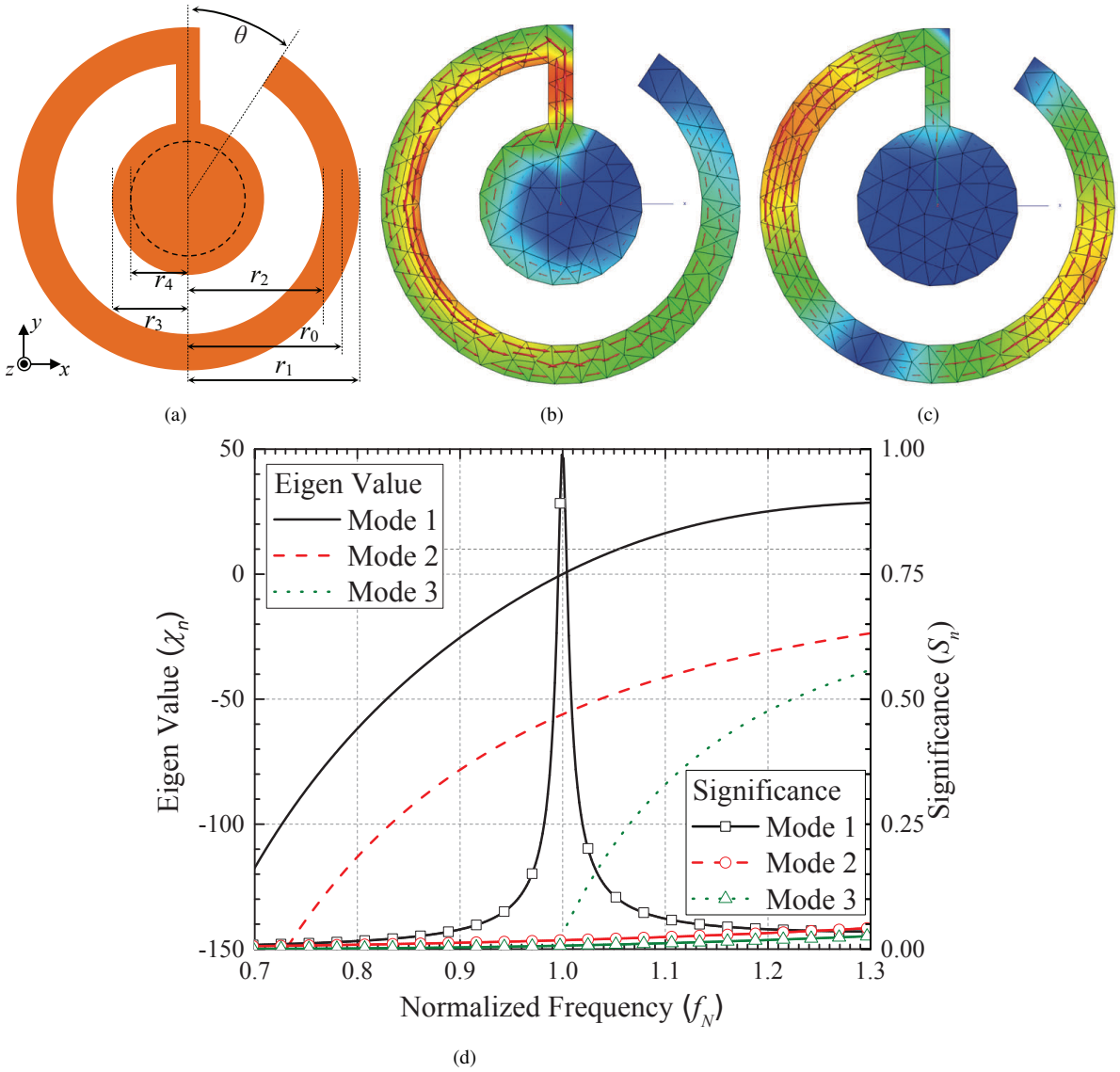

Fig. 1. *(a) The proposed planar circular radiating body with a disk ground plane transformed from a monopole, (b) current flow of mode 1, (c) current flow of mode 2, and (d) eigen values λ_n and modal significance S_n for its first three modes.*

A generic model of the proposed radiating body is established and simulated in the commercial software package FEKO to carry out the CMA. Modal current flows of the first two significant eigen modes are illustrated in Fig. 1(b) and (c). In Fig. 1(b), the modal current distribution of

mode 1 on the circular arm decreases gradually from the short end to the open end, which is similar to that of a typical monopole in its vertical form. However, there are two peaks in the current distribution of mode 2 as shown in Fig. 1(c). The mode 1 is therefore selected for the proposed circular radiating body.

The proposed radiating body should tune the resonant frequency of mode 1 at f_0 and suppress the higher modes. TCM implies that modes with eigen value $\lambda_n = 0\ (n = 1, 2, ...)$ are at resonance and radiate most efficiently [22]. Based on extensive CMA simulations, mode 1 can resonate at f_0 when the proposed radiating body is at settings of

$$\begin{aligned} r_1 : r_2 : r_3 : \lambda_0 &= 0.065 : 0.051 : 0.03 : 1 \\ \theta &= \pi/6 \end{aligned} \tag{1}$$

The effective length of the circular radiating body can be then defined as

$$l_e = \frac{r_0 + r_3}{2}(2\pi - \theta) \tag{2}$$

which is about $\lambda_0/4$ similar to a typical monopole.

Eigen values of the first three modes for the radiating body with settings in (1) are illustrated in Fig. 1(d), where frequency f is normalized to f_N using

$$f_N = f/f_0 \tag{3}$$

At $f_N = 1$, λ_1 is equal to 0 while λ_2 and λ_3 are far away from 0, which means that mode 1 is the most significant mode at the resonant frequency. This is consistent with modal current distribution shown in Fig. 1(b) and (c). The modal significance is another important quantity to compare the significance of each mode, and defined as

$$S_1 = \left| \frac{1}{1 + j\lambda_1} \right| \tag{4}$$

Corresponding modal significances of the first three modes are also illustrated in Fig. 1(d). At $f_N = 1$, S_1 is equal to 1 while λ_2 and λ_3 are very small and near 0. Therefore, it can be confirmed that the mode 1 should be the desired mode for the proposed radiating body.

2.2. Radiating bodies with different ring ground planes

In Fig.1(b), modal current on the disk are flowing mostly along the left edge. There is hardly current flow in the center and upper right area of the disk ground plane, which hints that the impact of current flow could be slight when these areas are removed. Fig. 2 illustrates three structures with different ring ground planes named as ***ring 1***, ***ring 2*** and ***ring 3***. ***Ring 1*** is formed by only removing the center area with a radius of r_4 from the disk. Simulations show that when $r_4 = 0.022\lambda_0$, the impacts on current flows between radiating body with disk and ring ground planes are slight. Based on ***ring 1***, ***ring 2*** is formed by removing the upper right part with arc of θ from the whole ring, while ***ring 3*** is formed by removing the upper left part with arc of θ from the whole ring.

As shown in Fig.2(a) and Fig. 2(b), the current flows on both ***ring 1*** and ***ring 2*** are in the opposite rotation direction to the current flows on the arm, which is the same as the radiating body with disk ground plane in Fig. 1(b). However, the current flow on ***ring 3*** is forced in the same rotation direction as the current flow on the circular arm when ***ring 3*** has an upper left cut, as

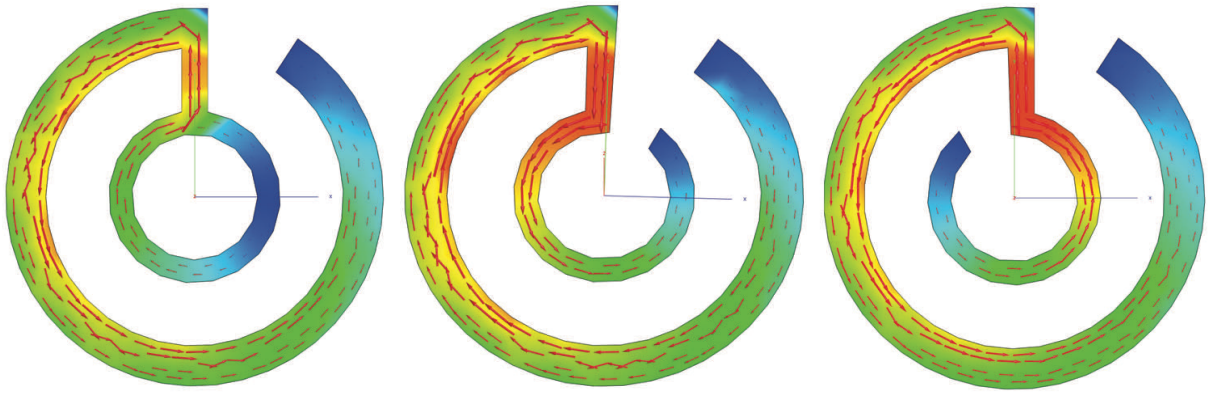

(a) (b) (c)

Fig. 2. *Structure with variant grounds and natural current flows of mode 1: (a)* ***ring 1****, (b)* ***ring 2*** *and (c)* ***ring3****.*

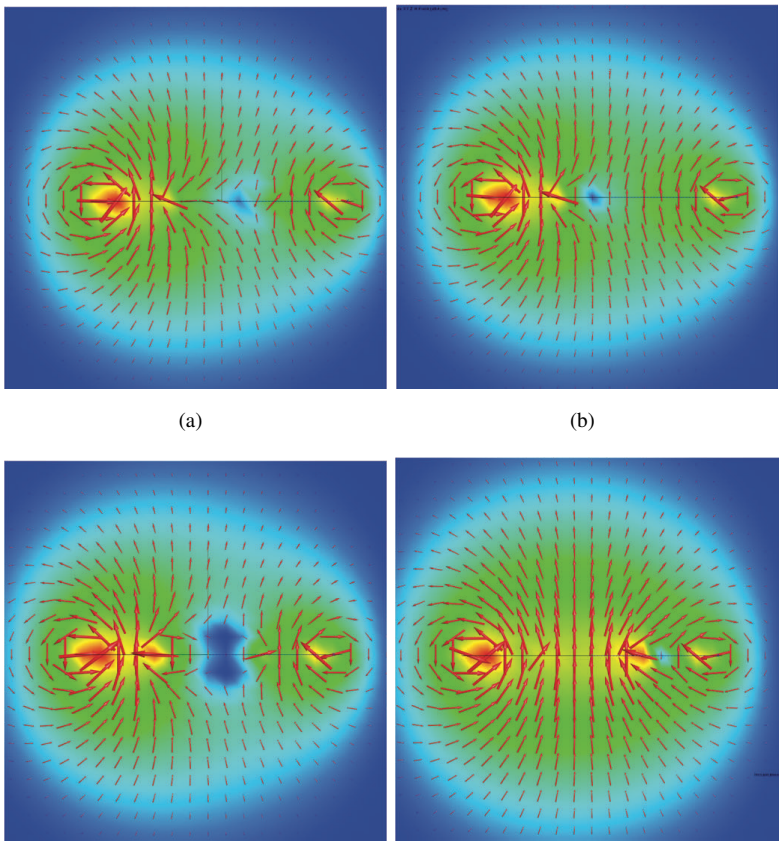

(a) (b)

(c) (d)

Fig. 3. *Near H-fields on xz-plane of mode 1 for radiating bodies with different ground planes: (a) disk, (b)* ***ring 1****, (c)* ***ring 2*** *and (d)* ***ring 3****.*

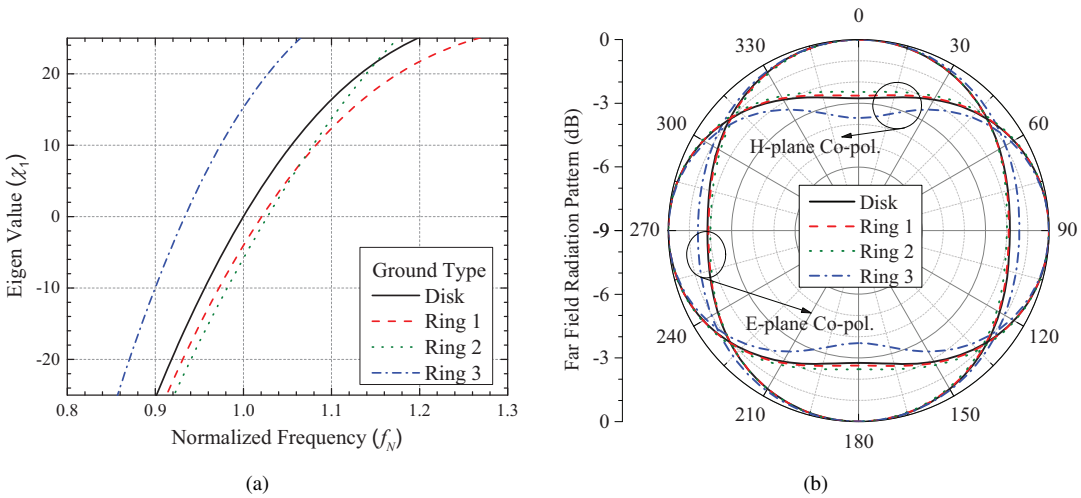

Fig. 4. *Comparison of radiating bodies with different ground planes: (a) eigen values λ_1 and (b) far field radiation patterns.*

shown in Fig. 2(c). With the cut on the ring being moved from right to left, the E-field between the arm and ***ring 3*** becomes more uniform, and the ***ring 3*** still serves as the ground plane.

Compared with ***ring 2***, the current flows on ***ring 3*** and the circular arm are in the same rotation direction, and therefore stronger and more uniform near H-field is generated, as shown in Fig. 3. H-fields in Fig. 3(a)-(c) are very similar, their magnitudes around the arm are strong while those around the center are weak. However, the H-field for ***ring 3*** in Fig. 3(d) is nearly uniform from the center to the outer edge of the structure. Thus, the radiating body with ***ring 3*** is more constructive and efficient.

Eigen value λ_1 for each ground plane is plotted in Fig. 4(a). Curves of λ_1 for ***ring 1*** and ***ring 2*** are on the right side and close to the one for the disk ground plane. This verifies again that the effect of cutting the central area of the disk ground plane is slight. The proposed radiating bodies with disk, ***ring 1*** and ***ring 2*** ground planes have similar radiation behaviors and resonant frequency. The blue dash-dot curve of λ_1 for ***ring 3*** is on the left side to the black solid curve for the disk, and both curves have similar trend except that there is a wide gap between them. This indicates that the radiating body with ***ring 3*** not only has the similar radiation behavior as the disk, but also supports lower resonant frequency.

Radiation patterns for the proposed radiating bodies with different ground planes are given in Fig. 4(b). Good agreements are observed in radiation patterns for different ground planes, especially for disk, ***ring 1*** and ***ring 2***. The radiation pattern for ***ring 3*** is slightly more omni-directional on E-plane than the one for other ground planes. These omni-directional radiation patterns in E-plane are primarily resulted from that their circular arm carries current flows with strong magnitudes, and the radiating body generates magnetic field lines passing through the most area surrounded by the circular arm as shown in Fig. 3.

With the aforementioned physical insight via CMA, the radiating body with ***ring 3*** is selected as the radiator for design of the antenna with a feeding structure.

Table 1 NORMALIZED RESONANT FREQUENCIES

***h* (Percentage of λ_0)**	0	0.15	0.30	0.45	0.60	1.20
Normalized resonant Frequencies (f_{Nc})	0.93	0.86	0.84	0.82	0.81	0.78

3. Proposed Circular Radiating Body with Magnetic Feeding Loop

3.1. Proposed radiator on substrate

Although the radiator can be realized by only one thin metal layer, it is more practical to fabricate it on the metal attached to the dielectric substrate by adopting PCB technologies. Therefore, substrate of Rogers 5880 with relative dielectric constant of $\epsilon_r = 2.2$ and height of h is used to model a practical design of the proposed radiator.

Value of h is swept to study the performance of radiators on dielectric substrates. The eigen values of radiators with different h are given in Fig. 5, indicating that the radiating body with a substrate has lowered resonant frequency. Thus, a smaller radiator can be achieved at the same frequency with existence of a substrate. The normalized resonant frequencies for different h are directly obtained from Fig. 5 and they are given in Table 1 as f_{Nc}

The proposed radiator can be generally designed at any desired resonant frequency with the aid of Table 1 and the geometric settings given in (1). Considering the tradeoff between very low

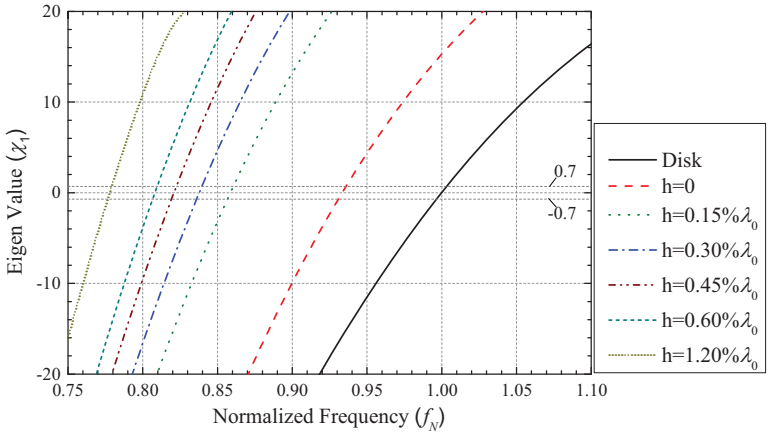

Fig. 5. *Eigen values λ_1 of radiators with substrates of different thicknesses represented by h in terms of λ_0.*

profile along z-axis and small size in xy-plane, substrate with height of $h = 0.6\%\lambda_0$ is selected for design of an example UHF radiator operating at its resonant frequency f_c=474MHz (λ_c=632mm). The radiator is designed through the following process:

First, according to (3), the reference resonant frequency f_0 can be determined by

$$f_0 = f_c / f_{Nc} \tag{5}$$

when f_c=474MHz and f_{Nc}=0.81 for $h = 0.60\%\lambda_0$ are replaced in (5), f_0=585MHz can be obtained.

Then, the corresponding wavelength is calculated as $\lambda_0 = c_0/f_0$=512mm, where c_0 is the light speed in free space;

Finally, according to (1), the geometric parameters of the example radiator are obtained as r_1=33mm (about $5.2\%\lambda_c$), r_2=26mm, r_3=15mm, r_4=11mm and h =3.1mm (about $0.5\%\lambda_c$).

3.2. Proposed Circular Antenna with magnetic feeding loop and its equivalent circuit

The CMA has been utilized to understand the proposed radiating body without considering exciting sources previously. It has been observed that the current flows on the proposed radiating body generate magnetic field lines passing through the most area surrounded by the circular arm. Given by TCM in [20], a modal solution for the current J on a conducting body defined by S in an impressed electric field E^i can be a linear superposition of the modal currents J_n, which is expressed as

$$J = \sum_n \frac{V_n^i J_n}{1 + j\lambda_n} = \sum_n \alpha_n J_n \tag{6}$$

where the modal excitation coefficient is

$$V_n^i = \oiint_s J_n \cdot E^i ds \tag{7}$$

When E^i is produced by a magnetic current M^i and reciprocal theorem is used to (7), we then have

$$V_n^i = -\iiint H_n \cdot M^i d\tau \tag{8}$$

where H_n is produced by a modal current J_n on S.

In xy-plane, a loop structure paralleled with the proposed radiating body is therefore able to generate normal direction equivalent magnetic current, which is in the same directions of the corresponding H-field generated by modal current J_1. Around the resonant frequency of mode 1 for the proposed radiating body, the eigen values of higher modes would be far away from zero. Also according to (6), if the small loop is placed near the strip connecting the inner ring and the outer circular arm, where the magnitude of the current flow of mode 1 is strongest and the one of mode 2 is weak, J_1 will be the only modal current with significant coefficient. Combining the radiator and magnetic feeding loop on different sides of the substrate, a planar circular antenna is illustrated in Fig. 6(a). A typical modal flow of mode 1 for the antenna with feed loop is also given in Fig. 6(b). It is clear that the rotation directions of current flows on the radiator and the feeding loop are opposite. This means the feeding loop and the radiator act as an air core transformer, which transfers the power from its feed port to the load by magnetic coupling. Hence, the feeding loop is named as the magnetic feeding loop in this paper.

Based on derivations in [20], when only J_1 is excited in the radiator and the radiated power is unit, the complex power balance for J_1 can be expressed as

$$P = 1 + j\lambda_1 \tag{9}$$

where j is the imaginary unit.

As shown in Fig. 5, eigen value λ_1 is nearly linear around the resonant frequency, and is zero at resonant frequency, negative below resonant frequency and positive above resonant frequency. This indicates that the frequency response of λ_1 is very similar to the one of reactance of a series

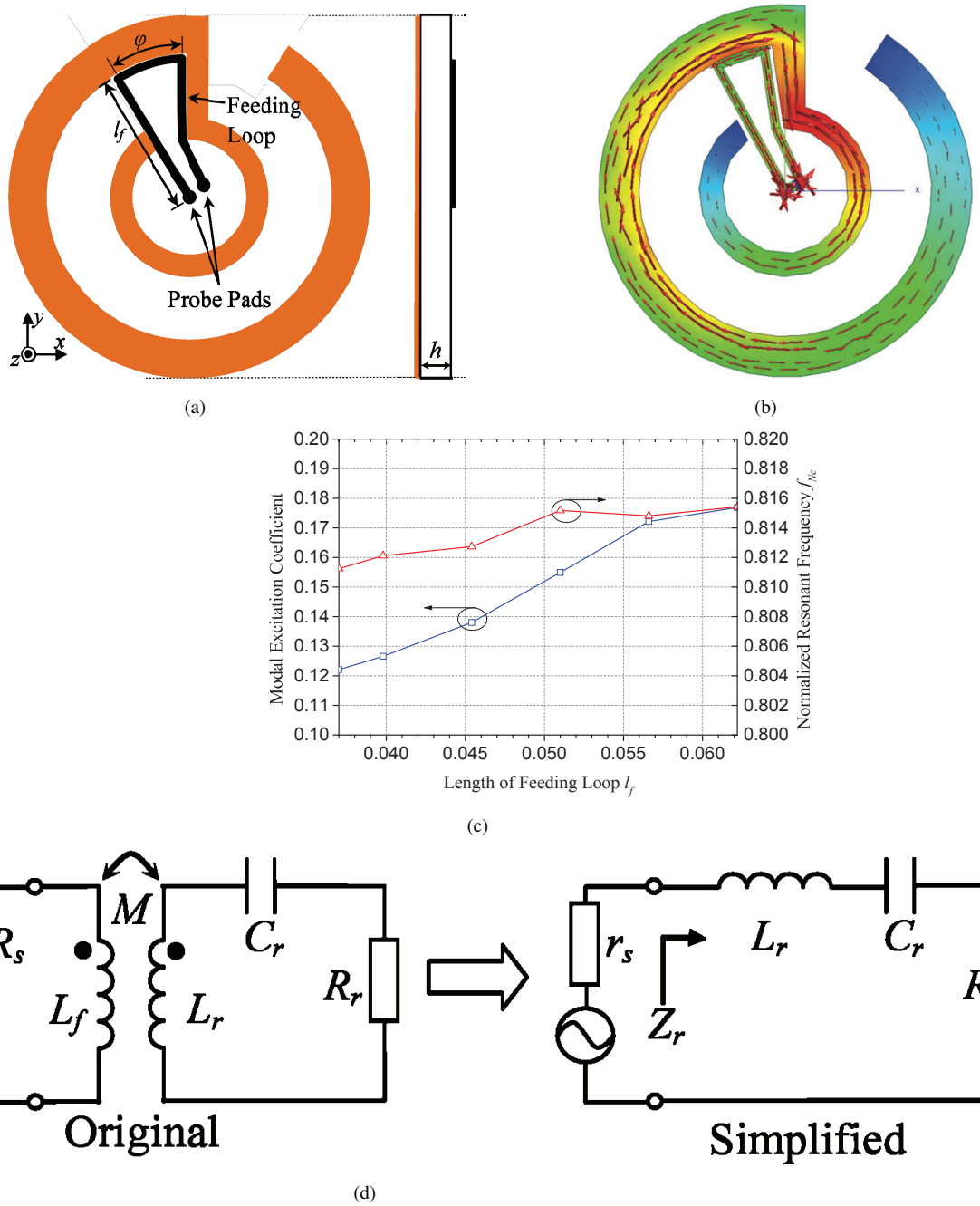

Fig. 6. *(a) Structure layout of the proposed circular antenna with magnetic feeding loop, (b) modal current flows of mode 1 for the antenna with feeding loop, (c) modal excitation coefficients and f_{Nc} with respect to the length of the feeding loop l_f, and (d) equivalent circuit of the proposed circular antenna with magnetic feeding loop.*

LC resonant circuit. Thus, the radiator can be represented by a series resonant circuit comprised of resistor R_r, inductor L_r and capacitor C_r [26]. The impedance of the series resonant circuit can be written as

$$Z_r = R_r + j\left(\omega L_r - \frac{1}{\omega C_r}\right) = R_r(1 + j\frac{X_r}{R_r}) \tag{10}$$

where X_r is used to simplify the imaginary part of Z_r. When the current provided by a source with efficient value of I flows through the series resonant circuit, the complex power balance in the circuit can be expressed as

$$P_e = Z_r I^2 = R_r I^2 (1 + j\frac{X_r}{R_r}) \tag{11}$$

In the case of the source providing unit power on R_r, i.e. $R_r I^2 = 1$, if $X_r/R_r = \lambda_1$ are satisfied, equation (11) and (9) are in the same form. Hence, the series resonant circuit becomes the equivalent circuit of the proposed radiator. In order to satisfy $X_r/R_r = \lambda_1$, R_r, L_r and C_r need to satisfy

$$\omega^2 L_r C_r - 1 = \lambda_1 \omega C_r R_r \tag{12}$$

which can be used to determine the values of L_r and C_r at the resonant frequency.

The main function of the magnetic feeding loop is to excite mode 1 to transfer the energy from source to the radiator, which is equivalent to realize the impedance matching between source and radiator excited in mode 1. The function can be realized by adjusting the size of the feeding loop. As shown in Fig. 6(a), the area of the feeding loop can be controlled by adjusting the length and radian of the feeding loop, indicating as l_f and ϕ. When $\phi = \pi/9$, the modal excitation coefficients (MEC) and normalized resonant frequency (f_{Nc}) of mode 1 with respect to l_f are extracted from a series of simulations. The results are given in Fig. 6(c). When l_f increases, resulting in the increase of the magnetic loop coupling area, MEC increases significantly, while f_{Nc} increases slightly. It means that MEC can be directly adjusted by l_f, and the effect of the feeding loop on the resonant frequency is small and can be neglected in the equivalent circuit for the sake of simplification. So, the small magnetic feeding loop can be used as the excitation structure and its inductance L_f is much less than L_r, and therefore the effect of L_f on the resonant frequency of the radiator is ignored.

Now, the equivalent circuit of the proposed antenna combining the radiator and magnetic feeding loop is given in Fig. 6(d). Considering the voltage and impedance transformation of the magnetic feeding loop just like the primary coil in an air transformer, the load effect of source impedance R_s can be transformed into the series resonant circuit of the radiator as r_s, so the original equivalent circuit is transformed into the simplified one as Fig. 6(d) shows.

If impedance matching between source and radiator are met at the resonant frequency, which can be realized by adjusting l_f, the relationship of $r_s = R_r$ must exist. Commonly, R_r nearly remains unchanged around the resonant frequency. Using (10) and (12), the reflection coefficient of the proposed circular antenna is derived as

$$\Gamma = \frac{Z_r - r_s}{Z_r + r_s} = \frac{Z_r - R_r}{Z_r + R_r} = \frac{\lambda_1}{\lambda_1 - j2} \tag{13}$$

3.3. Bandwidth estimation

For small antenna, the product of bandwidth and efficiency $B\eta$ is the most important performance indicator, and its theoretical limit for linearly polarized or single-mode antennas with $VSWR = 2$ is given in [3] as

$$B\eta = \frac{1}{\sqrt{2}} \left(\frac{1}{(kr)^3} + \frac{1}{kr} \right)^{-1} \tag{14}$$

where B is the fractional bandwidth with $VSWR = 2$, η is the radiation efficiency, k is the wave number and r is the radius of the smallest sphere enclosing the antenna.

Table 2 ESTIMATED FRACTIONAL BANDWIDTHS

***h* (Percentage of λ_0)**	0	0.15	0.30	0.45	0.60	1.20
Fractional bandwidth(%)	0.55	0.46	0.42	0.4	0.38	0.34

Replacing Γ in the relationship of $VSWR$ and Γ with the expression given in (13), the VSWR of the antenna can be derived as

$$VSWR = \frac{1+|\Gamma|}{1-|\Gamma|} = \frac{\sqrt{\lambda_1^2+4}+|\lambda_1|}{\sqrt{\lambda_1^2+4}-|\lambda_1|} \tag{15}$$

Using the condition of $VSWR = 2$ to (15), we can obtain the solutions of λ_1 as

$$\lambda_1 = \pm\sqrt{2}/2 \approx \pm 0.7 \tag{16}$$

λ_1 is a function of frequency, once it is obtained by CMA two horizontal lines with constant values of -0.7 and 0.7 cut a certain curve of λ_1 at two normalized frequency points denoted as f_{Nl} and f_{Nh}, respectively as shown in Fig. 5 for example. Then, the fractional bandwidth is estimated as

$$B = (f_{Nh} - f_{Nl})/f_{Nc} \tag{17}$$

Reading from Fig. 5, the estimated fractional bandwidths for different h are evaluated and given in Table II.

4. Simulated and Measurement Results and Analyses

An example of the proposed circular antenna operating at 474MHz is also modeled and simulated in software CST microwave studio with parameters of r_1=33mm, r_2=26mm, r_3=15.5mm, r_4=11.5mm and h=3.1mm. The antenna is fabricated and measured at Queen Mary University of London. The prototype is shown in Fig. 7(a) and (b). A customized SMA connector is soldered on the probe pads through holes.

Fig. 7(c) presents the VSWR and total efficiency of the proposed antenna. Resonant frequency and $VSWR < 2$ bandwidth are about 474MHz and 2.2MHz in simulation, and 471MHz and 3.3MHz for measurement. The simulated total efficiency is 84% at 474MHz. The measured VSWR has a lower center frequency and a wider bandwidth than the simulated one. The radiation patterns of the proposed antenna is also simulated by CST and given in Fig. 7(d). Its clear that the radiation patterns of the proposed antenna agree well with the ones of the radiator given by CMA. This means the radiation patterns of the CMA can be used to predict the radiation behavior of the proposed antenna.

As shown in Fig. 7(a), the antenna prototype is measured with a SMA connector and test cable, which generally affects the near field around the radiating body for such a UHF band compact antenna with small ground structure although calibration is carried out. Cables with different lengths of l are located in the center of the proposed radiator shown in Fig. 7(a) and (b). The corresponding λ_1 are obtained and shown in Fig. 8(a). It can be observed that the resonant frequency of the antenna decreases when the length of cable increases. When $l < (\lambda_c/8)$, only resonant frequency decreases slightly while the fractional bandwidth remains unchanged, reflecting by the unchanged

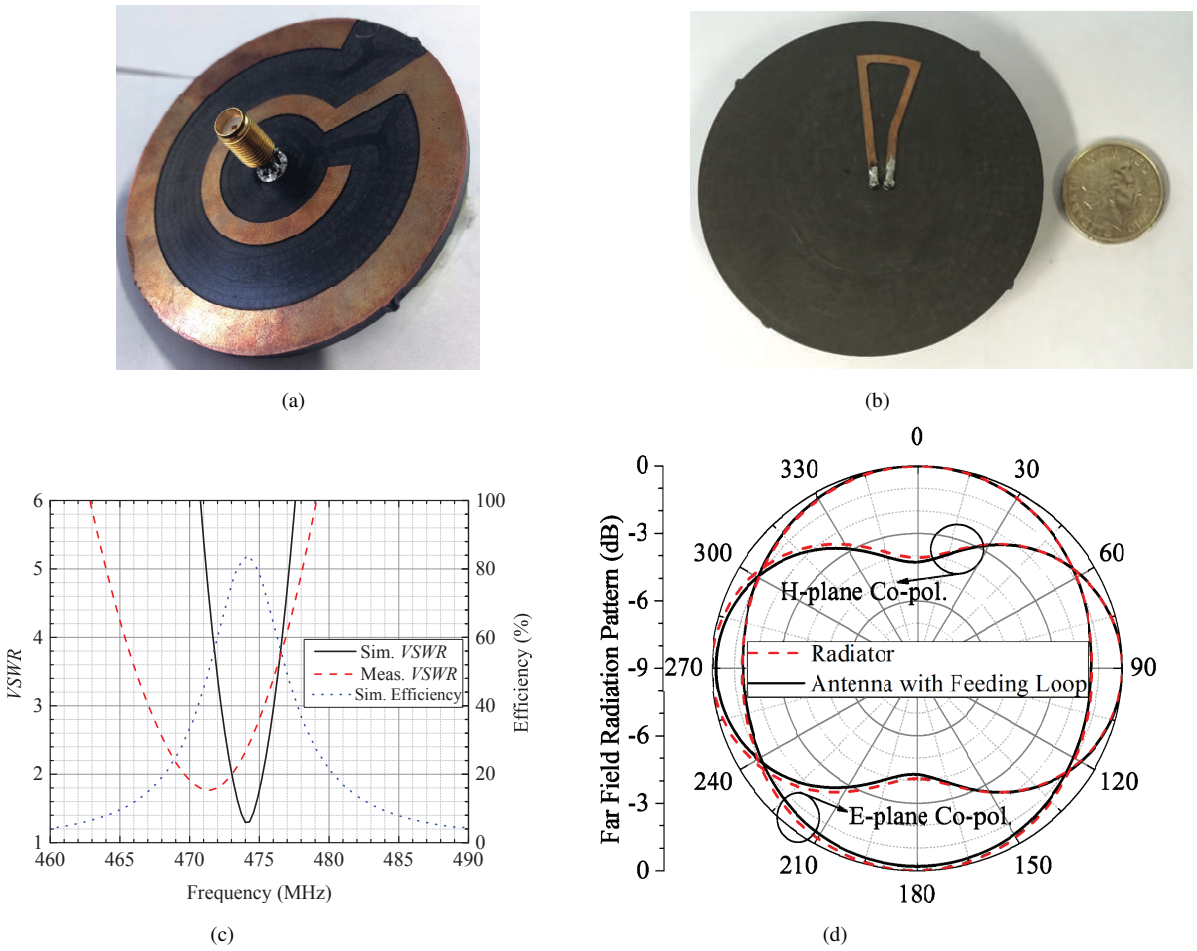

Fig. 7. *Prototype of the proposed circular antenna: (a) radiator side view and (b) magnetic feeding loop side view. (r_1=33mm, r_2=26mm, r_3=15.5mm, r_4=11.5mm and h=3.1mm corresponding to parameters in Fig. 1(a)), (c) VSWR and total efficiency of the proposed antenna, and (d) radiation patterns.*

slope around the resonant frequency. When $l > (\lambda_c/4)$, resonant frequency still decreases while the fractional bandwidth begins to increase, because the slope around the resonant frequency decreases. When $l \approx (\lambda_c/2)$, the cable becomes a dipole with strong radiation at the operating frequency, it will strongly affect the desired radiation mode of the proposed small antenna. So, the proposed circular antenna can keep its performance for compact devices without a feeding cable, e.g. directly connecting to a small sensor.

In order to evaluate the performance of the proposed circular antenna, the relevant performance data versus kr of various antennas are illustrated in Fig. 8(b). The antennas for comparison purposes include the proposed antennas with different thickness of the substrate h, an ideal dipole with same kr and resonant frequency as the proposed prototype, and several small antennas reported in the open literature. The performance data contain $B\eta$ of each compared antenna, ratio of $B\eta$ of each antenna to the theory limit with same kr, experimental limit of $B\eta$ for planar antennas which is defined by the best planar antennas cited in the literature [3], and are named as $(B\eta)_a$, $(B\eta)_L$, $(B\eta)_a/(B\eta)_L$ and $(B\eta)_E$, respectively.

In Fig. 8(b), solid and hollow symbols with same kr represent $(B\eta)_a$ and $(B\eta)_a/(B\eta)_L$ of the

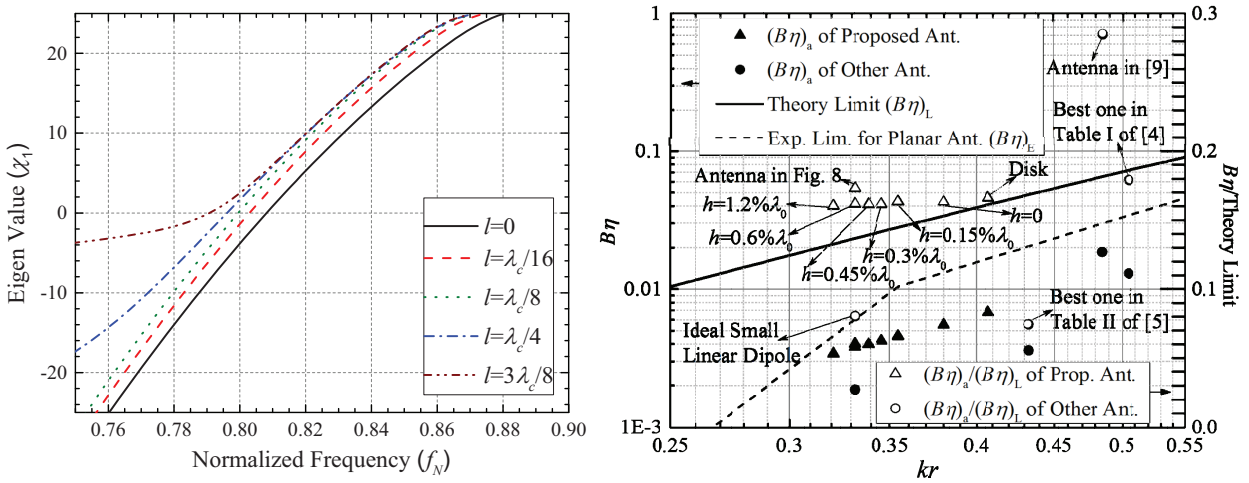

Fig. 8. *(a) Eigen value λ_1 of the proposed circular radiator with a test cable at different lengths and (b) comparison of $(B\eta)$ and $(B\eta)$/(Theory Limit) between the proposed and other antennas.*

same antenna. $(B\eta)_a$ labelled with $h = p\lambda_0$ are directly based on Table 2 , where p is a percentage. The change trend of gap between $(B\eta)_L$ and $(B\eta)_E$ reflects that the smaller kr is, the more difficult the design of planar small antenna is. $(B\eta)_a/(B\eta)_L$ of the proposed antennas are not as high as the antennas in [9], but corresponding to smaller kr. All $(B\eta)_a$ are below the polyline defined by $(B\eta)_E$. For the proposed antenna, the thicker the substrates is, the closer $(B\eta)_a$ to $(B\eta)_E$ is. Changes of $(B\eta)_a/(B\eta)_L$ of the proposed antennas are very small when the height of substrate increases. It implies that the proposed antenna is suitable for very small antenna designs and has the potential to extend the experimental limit for planar antenna when the antenna is fabricated on substrate with high relative dielectric constant and height.

It is worth mentioning that $(B\eta)_a$ of the antenna in Fig. 7(a) is based on results of the model with the same parameters as the prototype and a SMA connector simulated in CST, and it is a little larger than the estimated one (corresponding to $h = 0.6\%\lambda_0$) due to the existence of feeding structure and SMA connector. Therefore, the derived bandwidth estimation in this paper is verified and can be generally used, being faster than EM simulations as it only needs the information of λ_1 with respective to frequency provided by CMA.

5. Conclusions

The paper presented a very low profile circular UHF small antenna with radiating body transformed from a monopole. Characteristic mode analysis (CMA) was used to analyze and design the proposed antenna. After the comparison of radiation behaviors and sizes of several radiating bodies with different ground planes, the one with an improved ring ground plane was selected as the radiator for the proposed antenna. The omni-directional radiation patterns of the radiator were achieved on E-plane due to the natural almost full-round current flow of mode 1. CMA pointed out that the size of radiator fabricated on a substrate can be smaller than the one with only conductor, and the normalized resonant frequency for the radiator fabricated on substrate was a scale factor of the geometric length. A magnetic feeding loop was integrated with the radiator to construct the proposed small antenna, where an equivalent circuit was established and used to estimate its

bandwidth based on the physical insight of CMA.

An example of the proposed low profile circular antenna was practically designed and fabricated at 474MHz with a radius of 33mm ($5.2\%\lambda_c$, λ_c is the operating frequency wavelength), and a profile of 3.1mm ($0.5\%\lambda_c$). There was a discrepancy between simulated and measured VSWR of the prototype. The CMA of the proposed antenna with a test cable at lengths was applied to exam the difference. Based on the analysis and performance evaluation, the proposed antenna can be a strong contender for compact sensors at UHF TV white space for M2M and IoT applications.

Acknowledgement

The authors would like to acknowledge the Engineering and Physical Sciences Research Council (EPSRC) in the UK for their support of this work with Grant No. EP/L024241/1. The authors would also like to thank the Natural Science Foundation of Shanxi Province (2015011051).

6. References

[1] H. A. Wheeler, "Fundamental limitations of small antennas," *Proc. IRE*, vol. 35, pp. 1479-1484, 1947.

[2] L. J. Chu, "Physical limitations of omni-directional antennas," *J. Appl. Phys.*, vol. 19, pp. 1163-1175, 1948.

[3] D. F. Sievenpiper, D. C. Dawson, M. M. Jacob, T. Kanar, S. Kim, J. Long, and R. G. Quarfoth, "Experimental validation of performance limits and design guidelines for Small antennas," *IEEE Trans. Antenna Propag.*, vol. 60, no. 1, pp. 8-19, 2012.

[4] W. Hong and K. Sarabandi, "Low-profile, multi-element, miniaturized monopole antenna, "*IEEE Trans. Antenna Propag.*, vol. 57, no. 1, pp. 72-80, 2009.

[5] J. Oh and K. Sarabandi, "Low Profile, Miniaturized, Inductively Coupled Capacitively Loaded Monopole Antenna," *IEEE Trans. Antennas Propag.*, vol. 60, no. 3, pp. 1206-1213, 2012.

[6] S. S. Aljaafreh, Y. Huang, L. Xing, "A Compact, Wideband and Low Profile Planar Inverted-L Antenna," *EuCAP 2014, Hague*, pp. 3283-3286, 2014.

[7] G. Zamora, S. Zuffanelli, F. Paredes, F. Martaín and J. Bonache, "Design and Synthesis Methodology for UHF-RFID Tags Based on the T-Match Network," *IEEE Trans. Microwave Theory Tech.*, vol. 61, no. 12,pp. 4090-4098, 2013.

[8] G. Zamora, F. Paredes, F. J. Herraiz-Martínez, F Martín and J. Bonache, "Bandwidth limitations of ultra high frequency-radio frequency identification tags," *IET Microwaves, Antennas & Propag.*, vol. 7, no. 10, pp. 788-794, 2013.

[9] Y. Saita, N. Kagiyama, T. Ito, and H. Morishita, "Fundamental characteristics of a circular combined folded dipole antenna with a feed line," *AP-S/URSI 2014, Memphis, TN, USA*, pp. 1101-1102, 2014.

[10] P. Kolodzy and I. Avoidance, "Spectrum policy task force," *Federal Commun. Comm., Washington, DC, Rep. ET Docket*, no. 02-135, 2002.

[11] *UK Office of Communications (Ofcom)*, Statement on Cognitive Access.

[12] O. Holland, S. Ping, Y. Gao, Z. Qin, A. Aijaz, J. Chareau, P. Chawdhry, and H. Kokkinen, "To white space or not to white space: That is the trial within the ofcom TV white spaces pilot", *in the IEEE International Symposium on Dynamic Spectrum Access Networks (DYSPAN), Stockholm, Sweden*, Sep. 2015. (To appear)

[13] Z. Qin, Y. Gao, M. Plumbley, and C. Parini, "Efficient compressive spectrum sensing algorithm for M2M devices," *in IEEE Global Conference on Signal and Information Processing (GlobalSIP) Symposium on Cognitive Radios and Networks*, pp. 1170-1174, Atlanta, Dec. 2014.

[14] M. Dohler and Y. Gao, Chapter "Spectrum to Unlash Machine-to-Machine Uptake," *in the Wiley book "Opportunistic Spectrum Sharing and White Space Access: The Practical Reality"*, May 2015.

[15] Y. Ma, Y. Gao and C. G. Parini, "Sub-Nyquist Rate Wideband Spectrum Sensing over TV white space for M2M Communications," *the IEEE WoWMoM, Boston, USA*, Jun. 2015.

[16] Y. Gao, R. Ma, Q. Zhang and C. Parini, "UHF antennas for Machine-to-Machine communications and Internet Of Things," *EuCAP 2015, Davos*, pp. 1-3, Apr. 2016.

[17] R. Ma, Y. Gao, Y. Wang and C. Parini, "Circular Co-Planar Inverted-F Antenna for UHF Machine-to-Machine Communications," *AP-S/URSI 2015, Vancouver*, pp. 1418-1419, Jul. 2015.

[18] Q. Zhang, Y. Gao and C. G. Parini, "Miniaturized UHF Antenna Using a Magneto-dielectric Superstrate for M2M Communications," *AP-S/URSI 2015, Vancouver*, Jul. 2015.

[19] R. J. Garbacz and R. H. Turpin, "A generalized expansion for radiated and scattered fields," *IEEE Trans. Antennas Propag.*, vol. 19, no. 3, pp. 348-358, 1971.

[20] R. F. Harrington and J. R. Mautz, "The Theory of Characteristic Modes for Conducting Bodies," *IEEE Trans. Antennas Propag.*, vol. 19, no. 5, pp. 622-628, 1971.

[21] R. F. Harrington and J. R. Mautz, "Computation of characteristic modes for conducting bodies," *IEEE Trans. Antennas Propag.*, vol. 19, no. 5, pp. 629-639, 1971.

[22] M. Vogel, G. Gampala, D. Ludick, U. Jakobus and C. J. Reddy, "Characteristic Mode Analysis: Putting Physics back into Simulation," *IEEE Antennas Propag. Magazine*, vol. 57, no. 2, pp. 307-317, 2015.

[23] Z. Miers, H. Li, and B. K. Lau, "Design of Bandwidth-Enhanced and Multiband MIMO Antennas Using Characteristic Modes," *IEEE Antennas Wireless Propag. Lett.*, vol. 12, pp. 1696-1699, Nov. 2013.

[24] Y. Chen and C. F. Wang, "Electrically small UAV antenna design using characteristic modes," *IEEE Trans. Antennas Propag.*, vol. 62, no. 2, pp. 535-545, 2014.

[25] D. Manteuffel, "Characteristic Mode based antenna design - A straight forward approach to small form factor antenna integration," *EuCAP 2015, Lisbon, Portugal*, pp.1-5, Mar. 2015.

[26] R. Ludwig and P. Bretchko, RF Circuit Design - Theory and Applications, *Prentice Hall,* pp. 210-217, 2000.